

Assembly and performance of hybrid-VRLA cells and batteries

S.K. Martha^{a,*}, B. Hariprakash^a, S.A. Gaffoor^b, S. Ambalavanan^c, A.K. Shukla^{a,c}

^a Solid State and Structural Chemistry Unit, Indian Institute of Science, Bangalore 560012, India

^b NED Energy Ltd., 6-3-1109/1 Navbharat Chambers, Raj Bhavan Road, Hyderabad 500082, India

^c Central Electrochemical Research Institute, Karaikudi 630006, India

Abstract

Several commercial-grade hybrid-VRLA and AGM-VRLA cells and batteries have been assembled and tested under varying charge–discharge rates in a temperature range between 50 and -40°C . Impedance studies on hybrid-VRLA and AGM-VRLA cells have been conducted to reflect on their resistive and capacitive values. A linear relationship is found to exist between logarithmic state-of-charge values and ohmic impedance of batteries. In general, hybrid-VRLA cells and batteries perform better than their AGM-VRLA counterpart. A field-performance study conducted on AGM-VRLA and hybrid-VRLA batteries for solar-lighting application also suggests the latter to be superior.

Keywords: VRLA batteries; Absorbent-glass-mat (AGM); Gelled electrolyte; Colloidal silica; Hybrid; Oxygen recombination

1. Introduction

The lead–acid battery is one of the most successful electrochemical systems ever developed, and no other battery is yet able to compete with the lead–acid batteries on cost grounds, albeit batteries based on other chemistries are rapidly catching up [1]. In the past, although lead–acid battery designs have been optimized in several different ways, there are still certain new challenges facing the lead–acid battery designers as additional failure modes have become evident in various use modes [2–5].

There are three types of lead–acid batteries in common use: (a) batteries with flooded or excess electrolyte, (b) low-maintenance lead–acid batteries with a large excess of electrolyte, and (c) batteries with immobilized electrolyte and a pressure-sensitive valve usually referred to as absorptive glass-microfibre (AGM) valve-regulated lead–acid (VRLA) batteries.

The flooded electrolyte lead–acid battery requires checking of specific gravity of the electrolyte, periodic addition of

water to maintain electrolyte above the plates, and recharge soon after the battery discharge to prevent hard sulfation, which affects the battery capacity. The emission of acid fumes causes corrosion of metallic parts in the vicinity of the battery, and the seepage of acid on the top cover of the battery could lead to a leakage current resulting in increased self-discharge and ground-shunt hazards. To overcome these problems, AGM-VRLA batteries based on oxygen-recombination cycle [6] have emerged. These batteries offer the freedom of battery placement, cyclability without the addition of water or checking the electrolyte specific gravity, increased safety, and superior performance in some instances [7].

Both flooded electrolyte [8–12] and AGM-VRLA [13–14] batteries can suffer from acid stratification. But AGM-VRLA batteries are especially susceptible to failures owing to the heat generated by oxygen recombination within the cells as well as due to cell-to-cell variations in electrolyte volumes [15–16]. Indeed, partial heating of AGM-VRLA batteries could cause dry-out with grid corrosion and even lead to thermal runaway [17–19]. Consequently, mitigating temperature variations in AGM-VRLA batteries are pivotal to their commercial success. The dissipation of local heat within the AGM-VRLA batteries can be achieved by adequately filling

* Corresponding author.

E-mail address: shukla@sscu.iisc.ernet.in (S.K. Martha).

the void volume in the battery with a thermally conducting gel, such as a gel formed from colloidal silica and sulphuric acid electrolyte. The AGM-VRLA and gelled electrolyte VRLA batteries have been combined to form the hybrid-VRLA battery version, which exhibits both the higher power density of AGM design and the improved thermal properties of the gel design [20–24].

Among various techniques employed for the characterization of VRLA batteries, impedance studies are known to provide several important battery performance parameters, such as ohmic resistance, charge-transfer resistance, double-layer capacitance, etc. [25–31], which are seminal: (a) to derive information on optimum utilization of the batteries, (b) to identify battery failure mode, and (c) to determine the state-of-charge (SoC)¹ of the batteries. In general, an electrochemical cell comprises resistive, capacitive and inductive components. The resistive component arises due to current collectors, electrolyte, bulk of the electrode materials, electron-transfer reactions at electrode/electrolyte interface, etc. The capacitive component arises due to double-layer capacitance while inductive component arises mainly due to porous nature of the electrodes. The total impedance of a cell comprises resistive and reactive components for the individual electrode processes. The high-frequency intercept of the semicircle provides the value of ohmic resistance (R_{Ω}), while the low-frequency intercept gives the value of charge-transfer resistance (R_{ct}).

As a part of our on-going research programme on VRLA batteries [32–38], in this communication, we report the assembly and performance characteristics of hybrid-VRLA cells and batteries in conjunction with their impedance studies. The study indicates that the discharge characteristics of the hybrid-VRLA cells and batteries are superior to AGM-VRLA cells and batteries over the operational temperatures between -40 and 50°C , although their impedance values are nearly similar. In a field-performance study conducted on the AGM-VRLA and hybrid-VRLA batteries for solar-lighting, the latter are found to be superior.

2. Experimental

2.1. Assembly of AGM-VRLA cells/batteries

AGM-VRLA (2 V/40 Ah) cells were assembled by stacking three positive plates each of 14 Ah and four negative plates each of 12 Ah. Positive and negative plates in these cells were separated by placing 2 mm AGM separator obtained from Nippon Sheet Glass Co., Japan. The plates were strapped with polythene bands and connected to their respective lugs. Prior to placing them in a polypropylene container, the cells were filled with the required amount of 5 M aqueous sulphuric acid and kept for 2 h for electrolyte soaking.

Monobloc AGM-VRLA (12 V/40 Ah) batteries were assembled by connecting six 2 V/40 Ah cells in series by group burning.

Industrial-grade 2 V/200 Ah AGM-VRLA cells were also assembled with four positive plates (each of 60 Ah) and five negative plates (each of 50 Ah) stacked alternately, which were wrapped with 2 mm AGM separator, and subsequently, strapped with polythene bands prior to placing them in a polypropylene container. The containers were filled with required amount of 5 M aqueous sulphuric acid and were kept for 2 h for electrolyte soaking. Both the AGM-VRLA cells and batteries were made positive limited to facilitate oxygen recombination at the negative plates.

2.2. Assembly of hybrid-VRLA cells/batteries

AGM-VRLA (2 V/40 Ah) cells were constructed as described in section 2.1, subjected to formation, and subsequently, filled with the required amount of gelled electrolyte obtained by ultrasonically mixing 5 M aqueous sulphuric acid with 5.5 wt.% colloidal silica procured from Eka Chemicals, Sweden. The hybrid-VRLA cells, thus assembled were kept for about 24 h for the gel to form fully and settle. As the gel stiffens, it shrinks and leads to formation of numerous micro-fine cracks. Monobloc (12 V/40 Ah) hybrid-VRLA batteries were assembled by connecting six 2 V/40 Ah cells in series by group burning. Hybrid-VRLA (2 V/200 Ah) cells were also assembled as described in section 2.1, and subsequent to their formation, were filled with the required amount of gelled electrolyte. Both the cells and batteries were made positive limited.

2.3. Formation and testing of cells/batteries

All the 2 V/40 Ah cells and 12 V/40 Ah batteries were formed over three cycles by charging them galvanostatically at C/10 rate followed by their discharge at C/5 rate using an automated Keithly 228A voltage/current source interfaced to a data acquisition system. Cells (2 V/200 Ah) were formed over three cycles by charging them galvanostatically at C/10 rate followed by their discharge at C/5 rate using a voltage/current source. The cells/batteries were charged/discharged at varying rates at temperatures ranging between -40 and 50°C in temperature-controlled chambers.

2.4. Impedance studies on 2 V/200 Ah hybrid-VRLA and AGM-VRLA cells

Impedance measurements at various state-of-charge (SoC) values of 2 V/200 Ah hybrid-VRLA and AGM-VRLA cells were carried out in the frequency range between 10 kHz and 5 mHz by employing an Autolab PGSTAT 30 instrument. The cells were discharged to various voltages and the SoC values for were fixed by taking 1.75 V as SoC = 0. The

¹ State-of-charge of a battery is the ratio between the available capacity at an instant to the total available capacity.

impedance parameters of the cells were evaluated from the experimental impedance spectrum employing an equivalent-circuit non-linear least square (NLLS)-fitting procedure due to Boukamp [39]. The NLLS-fit technique was employed using an appropriate equivalent-circuit with the circuit description code (CDC): $(RL) R (RQ) (RQ)$, where R , L , and Q stand for the circuit resistance, inductance and constant phase element, respectively. The elements within parentheses represent their parallel combination, while the elements without parentheses represent a series combination. The starting values were obtained from the Data Cruncher sub-program prior to using the values in the NLLS-fit program.

2.5. Self-discharge studies on 2 V/40 Ah hybrid-VRLA cells

Hybrid-VRLA cells (2 V/40 Ah) were stored for 30–90 days at 25 °C, and their discharge capacity values were obtained at C/5 rate using a Keithly 228A voltage/current source interfaced to a data acquisition system.

2.6. Cycle-life studies on 2 V/200 Ah and 12 V/40 Ah hybrid-VRLA cells/batteries

Cycle-life data on 2 V/200 Ah and 12 V/40 Ah hybrid-VRLA cells and batteries were obtained for about 200 cycles at 25 °C, using a Bitrode Model LCN cycle-life tester. For this purpose, the cells and batteries were discharged up to 1.75 V (SoC = 0) at 5 h (C/5) rate.

2.7. Studies on solar-lighting application of 12 V/40 Ah hybrid-VRLA and AGM-VRLA batteries

Both 12 V/40 Ah hybrid-VRLA and AGM-VRLA batteries were fitted separately to a street-lighting solar photovoltaic panel, which had two sub-panels, each comprising 36 silicon cells. The impedance of each sub-panel was 2.35 Ohms with V_{mp} (voltage at maximum power) = 17 V, I_{sc} (short-circuit current) = 2.5 A, and P_{max} (maximum power) = $40 \pm 10\%$. The energy in each of the batteries was used separately to light an 11 W CF lamp during the night hours. The batteries were charged during the day time with depth-of-discharge (DoD) varying between 25 and 30%. The percentage overcharge was found 3 to 9% more than the previous discharge. The batteries were installed in the first week of February 2004 and hourly data during battery charging was collected up to July 2004 using data loggers. Provision was also made to collect battery temperature (both ambient and cabinet), current, energy input, and intensity of solar radiation. All the experiments were conducted on a set of two batteries of each hybrid-VRLA and AGM-VRLA types. During the test period the lux was found to be vary between 86 and 106 $mW\ cm^{-2}$, while the temperature varied between 21 and 51 °C.

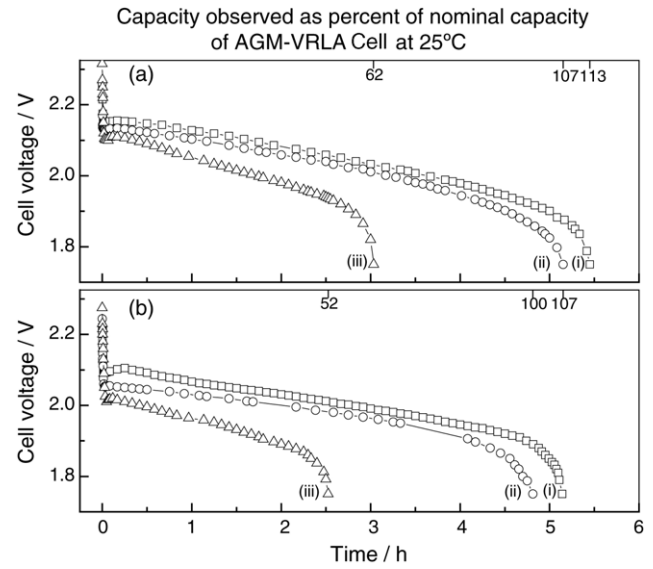


Fig. 1. Discharge capacity data for 2 V/40 Ah (a) hybrid-VRLA cells and (b) AGM-VRLA cells obtained at C/5 rate at (i) 50 °C, (ii) 25 °C, and (iii) –40 °C.

3. Results and discussion

Fig. 1a and b depict the comparison between discharge characteristics at 5 h (C/5) rate for the 2 V/40 Ah hybrid-VRLA and AGM-VRLA cells at 50, 25 and –40 °C, respectively. From the data, it is evident that the discharge capacity values for the hybrid-VRLA cells are higher than AGM-VRLA cells at all temperatures. The discharge data for 12 V/40 Ah hybrid-VRLA and AGM-VRLA batteries at various discharge rates at 25 °C, and their capacity values as percent of nominal capacity at C/5 rate are shown in Fig. 2a and b, respectively. We find that both the low-rate and high-rate discharge characteristics of the hybrid-VRLA batteries are superior to their AGM-VRLA counterpart. The data depicting the effect of temperature on the discharge characteristics of the 12 V/40 Ah hybrid-VRLA and AGM-VRLA batteries at C/5 rate are shown in Fig. 3a and b, respectively. Interestingly, the discharge capacity data for the hybrid-VRLA batteries exhibit improved performance in the entire temperature range between –40 and 50 °C in relation to AGM-VRLA batteries.

Discharge curves with varying rates obtained at 25 °C as percentage of the nominal capacity of the AGM-VRLA cells at 5 h (C/5) discharge rate for the industrial-grade 2 V/250 Ah hybrid-VRLA cells are shown in Fig. 4a, with the corresponding data for AGM-VRLA cells shown in Fig. 4b. From the data, it is clear that the capacities of hybrid-VRLA cells are 15–20% higher at low-discharge rates (C/10 to C/20) and 5–10% higher at high-discharge rates (C/5 to C) in relation to AGM-VRLA cells. In order to ascertain the field-performance reproducibility, a set of cells comprising 60 number of 2 V/200 Ah AGM-VRLA and 60 numbers of 2 V/250 Ah hybrid-VRLA cells have been discharged at C/10 rate concomitantly at 25 °C and the data are shown in Fig. 5a

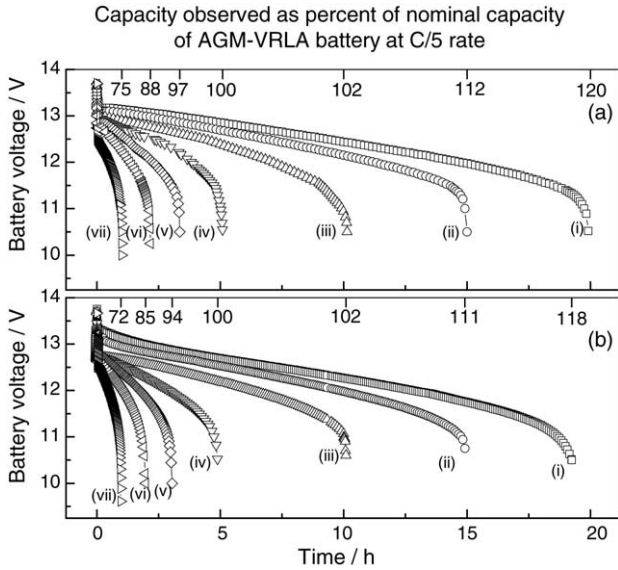


Fig. 2. Discharge capacity data for 12 V/40 Ah (a) hybrid-VRLA batteries and (b) AGM-VRLA batteries obtained at 25 °C at (i) C/20, (ii) C/15, (iii) C/10, (iv) C/5, (v) C/3, (vi) C/2, and (vii) C rates.

and b, respectively. From the data, it is clear that the performance of the hybrid-VRLA cells is superior to their AGM-VRLA counterpart.

The impedance spectra both for 2 V/200 Ah hybrid-VRLA and AGM-VRLA cells were obtained at various SoC values. A typical impedance spectra for the hybrid-VRLA and AGM-VRLA cells at SoC ~ 0.6 are shown as Nyquist plots in Fig. 6a and b, and respective Bode plots are shown in Fig. 7a and b. The Nyquist plot in Fig. 6a and b comprise an inductive distribution of the data at frequencies >0.057 kHz followed by two capacitive semicircles in the frequency range

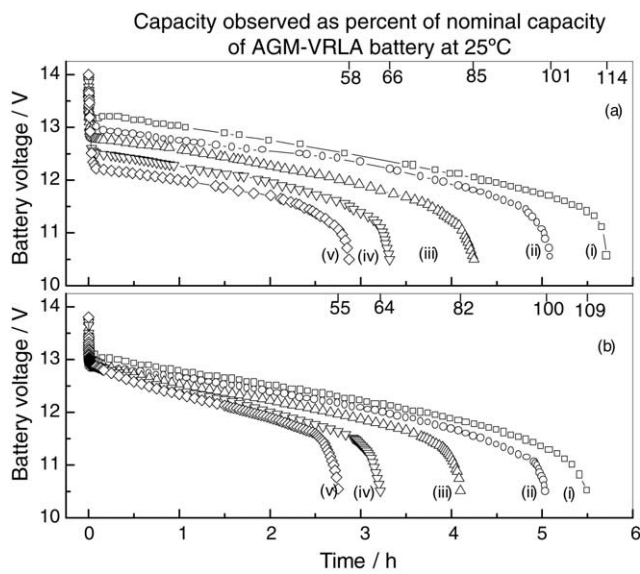


Fig. 3. Effect of temperature on the discharge capacities for 12 V/40 Ah (a) hybrid-VRLA batteries and (b) AGM-VRLA batteries at C/5 rate at (i) 50 °C, (ii) 25 °C, (iii) 0 °C, (iv) -20 °C, and (v) -40 °C.

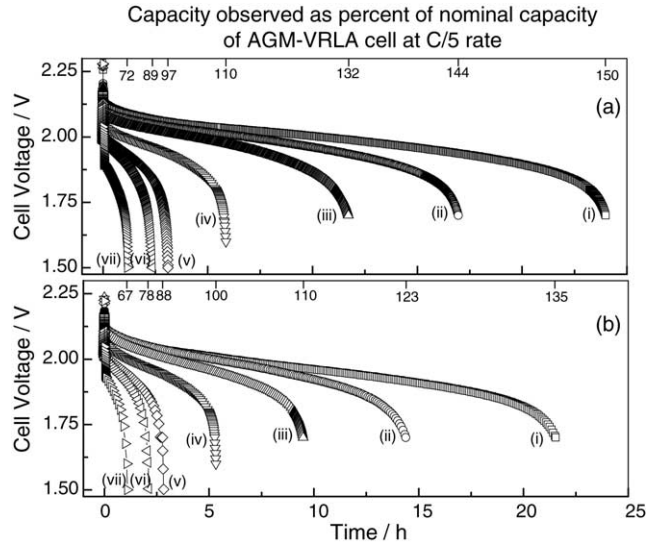


Fig. 4. Discharge capacity data for 2 V/200 Ah (a) hybrid-VRLA cells and (b) AGM-VRLA cells obtained at 25 °C at (i) C/20, (ii) C/15, (iii) C/10, (iv) C/5, (v) C/3, (vi) C/2, and (vii) C rates.

between 0.057 kHz and 5 mHz. The phase angle (ϕ) versus ac frequency plot in Fig. 7a and 7b suggest the value of ϕ to be positive at high frequencies, which corresponds to the inductive component of the cells. The phase angle gradually becomes negative with its peak value at -15° , reflecting the capacitive behavior of the battery in the frequency range between 0.057 kHz and 5 mHz.

The impedance parameters for AGM-VRLA and hybrid-VRLA cells were evaluated from the experimental impedance spectrum by an equivalent-circuit NLLS-fitting procedure due to Boukamp [39]. The equivalent-circuit, employed to fit the experimental data, is shown in Fig. 8. The high-frequency impedance data are inductive in nature as shown in Fig. 6 and could be fitted to a semicircle with the inductance (L)

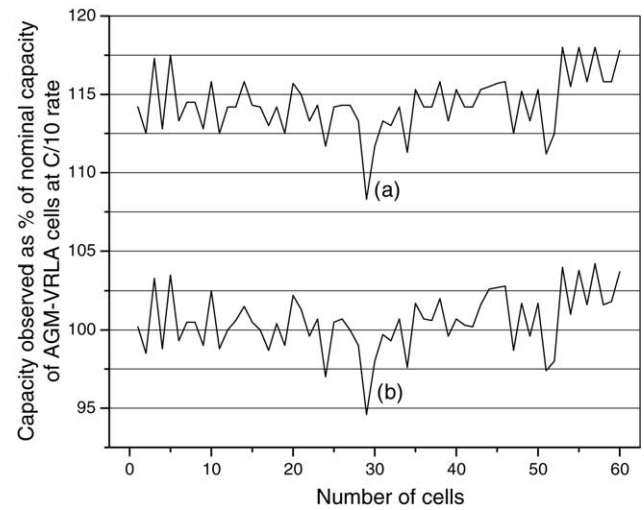


Fig. 5. Performance data obtained at 25 °C in % of nominal capacity at 10 h discharge rate for 60 industrial-grade 2 V/250 Ah (a) hybrid-VRLA cells and (b) AGM-VRLA cells.

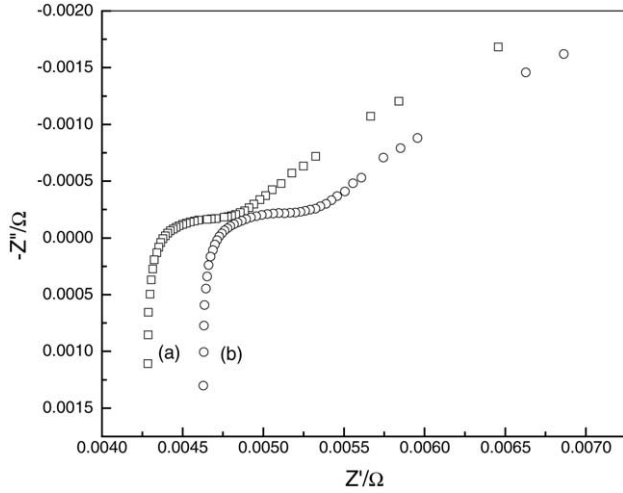


Fig. 6. Impedance spectrum for (a) hybrid-VRLA cell and (b) AGM-VRLA cell at SoC ~ 0.6 represented in Nyquist plot of imaginary part (Z''), vs. real part (Z').

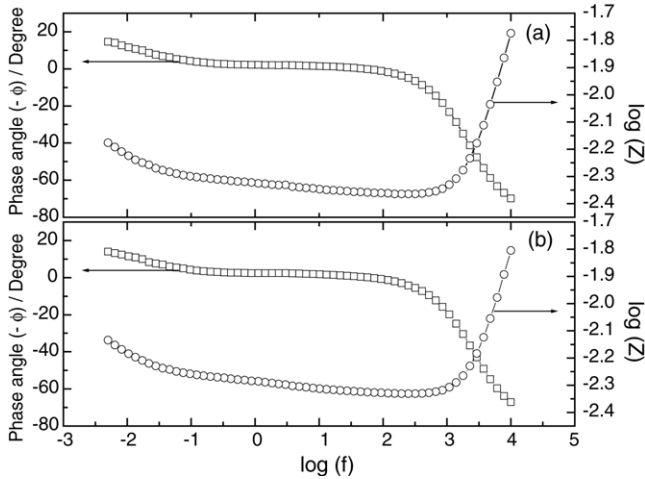


Fig. 7. Impedance spectrum for (a) hybrid-VRLA cell and (b) AGM-VRLA cell at SoC ~ 0.6 represented in Bode plot of logarithm of impedance ($\log Z$), and phase angle (ϕ) as a function of frequency (f).

and a resistance (R_L) in parallel. The elements R_Ω and R_1 represent the ohmic resistance and surface layer resistance, respectively; the charge-transfer resistance (R_{ct}) of the cell is represented by the second semicircle with frequency range between 57 and 5 mHz. The two capacitive semicircles are depressed, and more so is the high-frequency semicircle. Hence, a constant phase element (CPE) denoted as Q_1 is taken in parallel to a resistance R_1 corresponding to the high-frequency

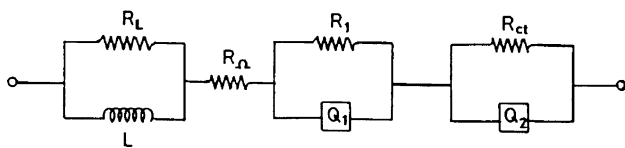


Fig. 8. Equivalent-circuit used for NLLS-fitting of experimental data of the VRLA cells.

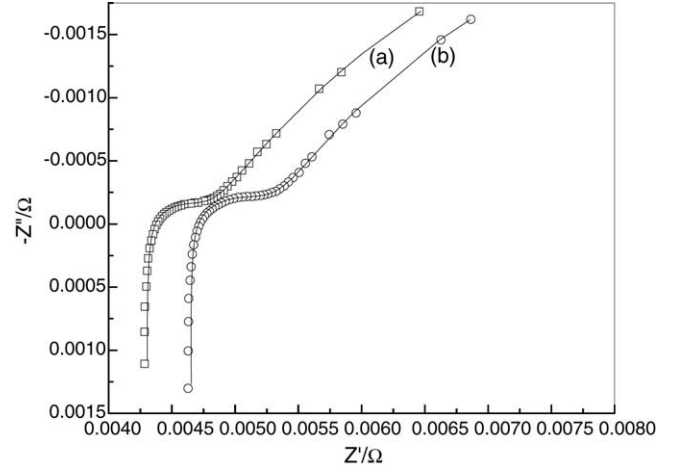


Fig. 9. Nyquist impedance spectra for the (a) hybrid-VRLA cells and (b) AGM-VRLA cells at SoC ≈ 0.6 at 25 °C. Experimental and simulated spectra from NLLS-fit are shown as symbols ($-\circ-$) and ($-\square-$) and as full lines, respectively.

semicircle while Q_2 is taken in parallel to R_{ct} . The CPE arises due to distribution of microscopic properties of the materials. Both the resistive and capacitive components of the electrode/electrolyte interface may change with the electrode position, non-uniform thickness of the electrode materials, etc. Owing to these factors, the semicircles in the Nyquist plots are depressed. The impedance plots comprising the experimental data points and the curves simulated from the fit parameters are shown in Fig. 9. A good agreement is seen between the experimental and the simulated data for all impedance representations.

The inductance behavior was attributed to the geometrical nature of conductors and electrodes, and not to the faradaic processes in the battery. Accordingly, the inductive distribution of the impedance of the lead–acid battery is due to the porous nature of the electrodes. The value for the inductance of the lead–acid cells was found to be about 2.5×10^{-7} H. The total impedance of the cell at SoC ~ 0 is found to be about 0.015Ω , which is well within the range of the resistance values reported for the lead–acid batteries [25]. The shunting resistance (R_L) across the inductance (Fig. 9) is only schematic, and is an artifact of the fitting procedure. The values of the inductance (L) and the shunting resistance (R_L), are therefore, considered irrelevant for characterizing the cells and these parameters have been omitted during the subsequent discussion. The fitting procedure was repeated after excluding the inductive dispersion of the impedance data, and L and R_L in the equivalent-circuit, while keeping the rest of the parameters unaltered. It was, thus confirmed that the inductance data did not influence the rest of the impedance spectrum. The resistance R_Ω is ascribed as the ohmic resistance of the battery, and includes the resistance of the electrolyte, current collectors, battery terminals, and inter-cell connectors. The values of R_Ω obtained from the NLLS-fit as well as from the high-frequency intercept of the Nyquist plot are found to be

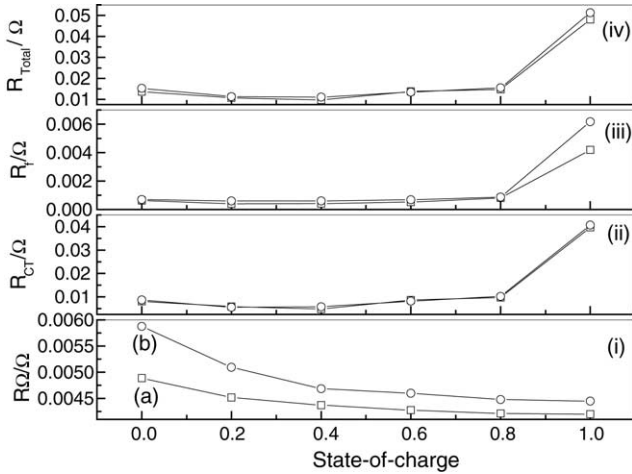


Fig. 10. The variation in impedance parameters (i) R_{Ω} , (ii) R_{ct} , (iii) R_1 , (iv) R_{Total} with state-of-charge for the (a) hybrid-VRLA cell (\square) and (b) AGM-VRLA cell (\circ).

nearly similar for both the hybrid-VRLA and AGM-VRLA cells (Fig. 10i).

In the literature [25–31], there is some inconsistency in assigning the capacitive semicircles to the respective electrodes of a battery. The charge-transfer resistance (R_{ct}) remains invariant for the SoC range between 0 and 0.8 but increases substantially for SoC values between 0.8 and 1 (Fig. 10ii). The values of R_{ct} are strikingly higher than the values of R_{Ω} (Fig. 10i) and R_1 (Fig. 10iii). The total cell resistance ($R_{Total} = R_{\Omega} + R_1 + R_{ct}$) values for the hybrid-VRLA and AGM-VRLA cells are shown in Fig. 10(iv). Although the ohmic, charge-transfer and surface-layer resistance values are different for hybrid-VRLA and AGM-VRLA cells, the total resistance values for both type of cells happen to be nearly similar over the entire SoC range. The ohmic resistance of the cells varies linearly with logarithmic values of their SoC as shown in Fig. 11,

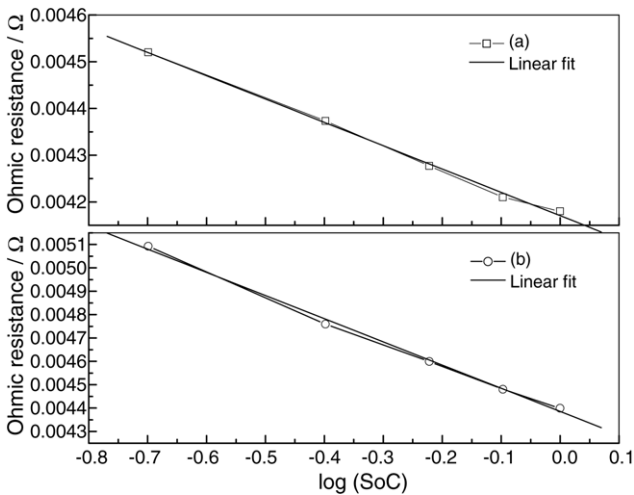


Fig. 11. Ohmic resistance values as function of $\log(\text{SoC})$ for (a) hybrid-VRLA cell and (b) AGM-VRLA cell at 25°C .

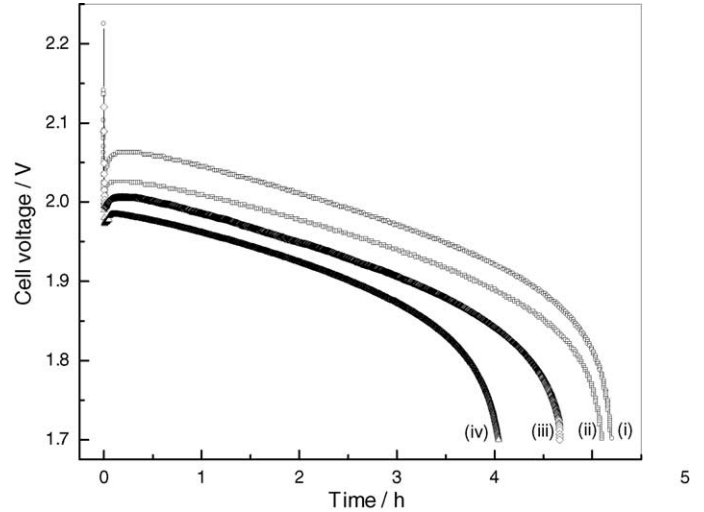


Fig. 12. Self-discharge data obtained at C/5 rate (i) before storage, (ii) 30 days of storage, (iii) 60 days of storage, and (iv) 90 days of storage for 2 V/40 Ah hybrid-VRLA cells.

and provides an attractive tool for monitoring of batteries [38].

In order to check the self-discharge values of the 2 V/40 Ah hybrid-VRLA cells, the cells were left standing for 30–90 days. From Fig. 12, it is seen that the hybrid-VRLA cells exhibit 2, 10, and 20% decay in their capacity after 30, 60, 90 days of storage, respectively, at 27°C . Under identical conditions, 2 V/40 Ah AGM-VRLA cells exhibited a capacity loss of about 5% after 30 days of storage.

The typical cycle-life data obtained both for the hybrid-VRLA 2 V/200 Ah cells and 12 V/40 Ah batteries at 25°C and C/5 rate are shown in Fig. 13i and ii, respectively. The data reflect a nominal loss of capacity 5% for both the hybrid-VRLA cells and batteries over 200 cycles is superior to their AGM-VRLA counterpart.

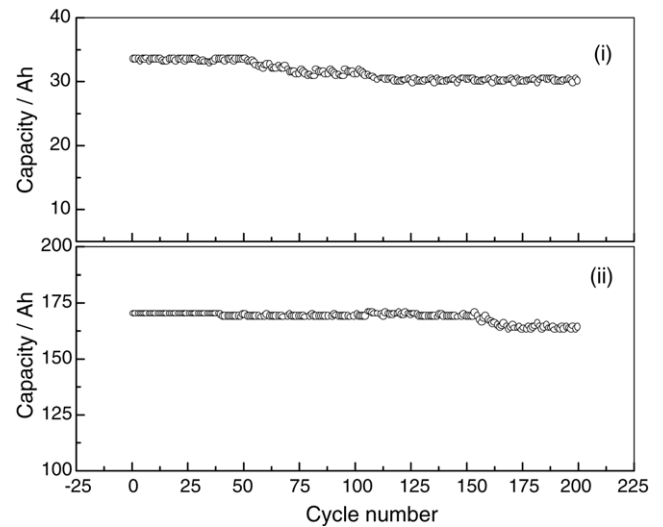


Fig. 13. Cycle-life data for hybrid-VRLA (i) batteries and (ii) cells obtained at C/5 rate at 25°C .

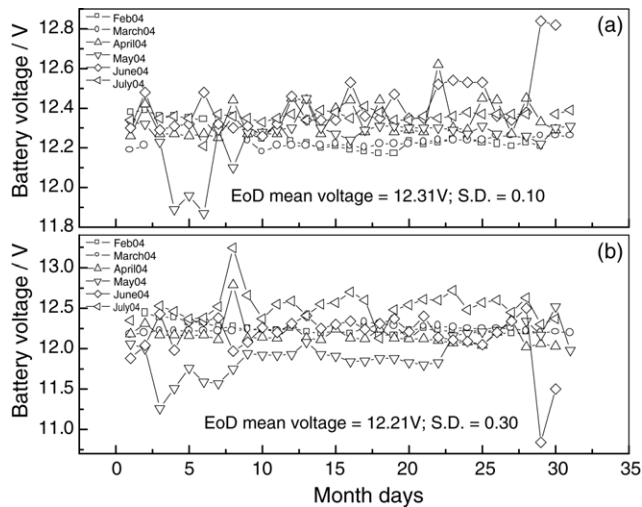


Fig. 14. End-of-discharge (EoD) voltage data for (a) hybrid-VRLA and (b) AGM-VRLA batteries during a solar street-lighting test application study conducted from February 2004 to July 2004. The mean values and respective standard deviations (S.D.) are also indicated.

During the field performance for solar-lighting application, the end-of-discharge (EoD) voltage data both for the hybrid-VRLA and AGM-VRLA batteries from February 2004 to July 2004 are shown in Fig. 14, the end-of-charge (EoC) voltage data for the hybrid-VRLA and AGM-VRLA batteries for the period February 2004 to July 2004 are shown in Fig. 15, and the data on variation in peak voltages of the hybrid-VRLA and AGM-VRLA batteries from February 2004 and July 2004 are shown in Fig. 16. A summary of the data in Figs. 14–16 is presented in Table 1.

From the data in Table 1, it is obvious that for the solar-lighting application field test conducted on the batteries from February 2004 to July 2004, (a) the respective mean values

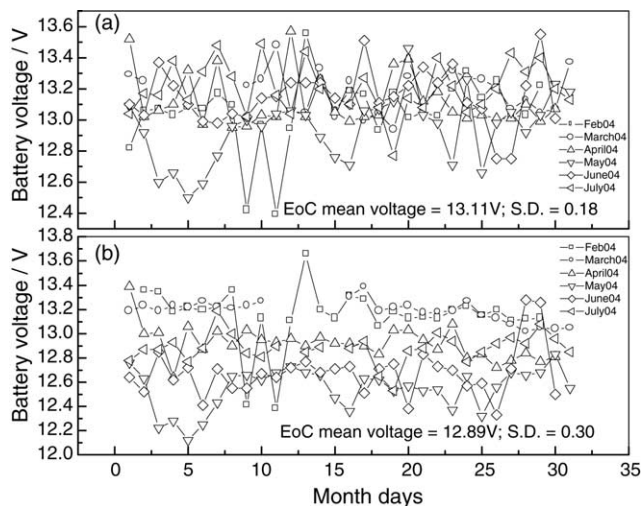


Fig. 15. End-of-charge (EoC) voltage data for (a) hybrid-VRLA, and (b) AGM-VRLA batteries during a solar street-lighting test application study conducted from February 2004 to July 2004. The mean values and respective standard deviations (S.D.) are also indicated.

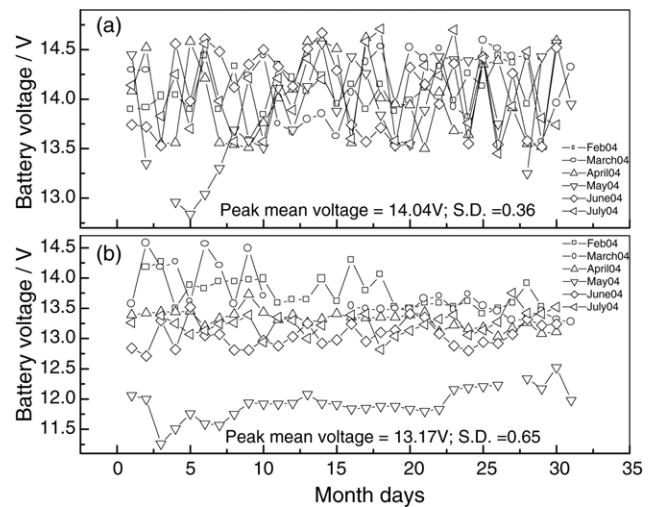


Fig. 16. Variation in peak voltages of the (a) hybrid-VRLA, and (b) AGM-VRLA batteries during a solar street-lighting test application study conducted from February 2004 to July 2004. The mean values and respective standard deviations (S.D.) are also indicated.

Table 1

Variation in mean values for the EoD, EoC and peak voltage values for 12 V/40 Ah hybrid-VRLA and 12 V/40 Ah AGM-VRLA batteries during the solar-lighting application test from February 2004 to July 2004

Parameters	Mean values	
	Hybrid-VRLA battery	AGM-VRLA battery
EoD voltage (V)	12.31	12.21
EoC voltage (V)	13.11	12.89
Peak voltage (V)	14.04	13.17

of the EoD voltages for the hybrid-VRLA and AGM-VRLA batteries are 12.31 and 12.21 V, (b) the respective mean values of the EoC voltages for the hybrid-VRLA and AGM-VRLA batteries are 13.11 and 12.89 V, and (c) the respective mean values of the peak voltages for the hybrid-VRLA and AGM-VRLA batteries are 14.04 and 13.17 V. These data clearly suggest a superior performance for the hybrid-VRLA batteries.

4. Conclusions

The study indicates that the deep discharge characteristics of the hybrid-VRLA cells and batteries are superior to AGM-VRLA cells and batteries over the operational temperatures between -40 and 50 °C. It is also found that the ac impedance spectrum of the VRLA cells comprises an inductive part and two capacitive components in the frequency range between 10 kHz and 5 mHz. The impedance parameters of the battery were obtained using a non-linear least square procedure. It is found that the impedance parameters corresponding to the low-frequency semicircle are useful for predicting SoC of the battery. The ohmic impedance values of the batteries vary linearly with the logarithmic state-of-charge value,

which appears to be a convenient method to monitor state-of-charge of the cells/batteries. The field trials for solar-lighting application conducted both on the AGM-VRLA and hybrid-VRLA batteries suggest the latter to be superior, presumably owing to their lower internal resistance.

Acknowledgement

We thank Mr. N. Gautam, NED Energy Ltd., Hyderabad for the kind encouragement and support during the course of this study.

References

- [1] R.M. Dell, D.A.J. Rand, *Understanding Batteries*, Royal Society of Chemistry, Cambridge, UK, 2002.
- [2] P.T. Mosely, *J. Power Sources* 95 (2001) 218.
- [3] A. Cooper, P.T. Mosely, *J. Power Sources* 113 (2003) 200.
- [4] K. Nakamura, M. Shiomi, K. Takahashi, M. Tsubota, *J. Power Sources* 59 (1996) 153.
- [5] D. Berndt, *J. Power Sources* 100 (2001) 29.
- [6] Y. Guo, J. Wu, L. Song, M. Perrin, H. Doering, J. Garche, *J. Electrochem. Soc.* 148 (2001) A1287.
- [7] D. Linden, T.B. Reddy (Eds.), *Handbook of Batteries*, third ed., McGraw- Hill, NY, 2002.
- [8] W.G. Sunu, B.R. Burrows, *J. Electrochem. Soc.* 128 (1981) 1405.
- [9] J. Richter, *J. Power Sources* 42 (1993) 231.
- [10] M. Shimpo, H. Nakashima, S. Sasabe, Y. Kasai, *Yuasa Jiho* 68 (1990) 26.
- [11] K. Takahashi, T. Sagawa, M. Tsubota, *GS News* 44 (1985) 8.
- [12] L. Apateanu, A.F. Hollenkamp, M.J. Koop, *J. Power Sources* 46 (1993) 239.
- [13] K. Higashimoto, A. Miura, T. Hayakawa, A. Komaki, *Prog. Batteries Solar Cells* 8 (1989) 268.
- [14] Y. Nakayama, T. Nagayasu, K. Kishimoto, Y. Kasai, *Yuasa Jiho* 71 (1991) 46.
- [15] A.L. Ferreira, H.A. Lingscheidt, *J. Power Sources* 67 (1997) 291.
- [16] D. Pavlov, *J. Power Sources* 48 (1994) 179.
- [17] R.J. Ball, R. Kurian, R. Evans, R. Stevens, *J. Power Sources* 109 (2002) 189.
- [18] R. Wagner, *J. Power Sources* 53 (1995) 153.
- [19] G.J. May, *J. Power Sources* 53 (1995) 111.
- [20] D.W.H. Lambert, P.H.J. Greenwood, M.C. Reed, *J. Power Sources* 107 (2002) 173.
- [21] S.D. Gerner, US Patent 5,376,479, 1994.
- [22] K.R. Bullock, *J. Power Sources* 116 (2003) 8.
- [23] S.S. Misra, T. M. Noveske, US Patent 4,863,816, 1989.
- [24] B.P. Varma, US Patent 4,317,872, 1982.
- [25] V. Viswanathan, A.J. Salkind, J.J. Kelley, J.B. Ockerman, *J. Appl. Electrochem.* 25 (1995) 729.
- [26] S. Rodrigues, Ph.D. thesis, Indian Institute of Science, Bangalore, India, 2001.
- [27] S. Rodrigues, N. Munichandraiah, A.K. Shukla, *J. Power Sources* 87 (2000) 12.
- [28] A. Salkind, T. Atwater, P. Singh, S. Nelatury, S. Damodar, C. Fennie Jr., D. Reisner, *J. Power Sources* 96 (2001) 151.
- [29] M.L. Gopikanth, S. Sathyanarayana, *J. Appl. Electrochem.* 9 (1979) 369.
- [30] M. Keddum, Z. Stoynov, H. Takenouti, *J. Appl. Electrochem.* 7 (1977) 539.
- [31] S.A.G.R. Karunathilaka, N.A. Hampson, R. Leek, T.J. Sinclair, *J. Appl. Electrochem.* 10 (1980) 357.
- [32] B. Hariprakash, P. Bera, S.K. Martha, S.A. Gaffoor, M.S. Hegde, A.K. Shukla, *Electrochem. Solid-State Lett.* 4 (2001) A23.
- [33] S.K. Martha, B. Hariprakash, S.A. Gaffoor, A.K. Shukla, *Bull. Mater. Sci.* 26 (2003) 465.
- [34] S.A. Shivashankar, A.K. Shukla, A.U. Mane, B. Hariprakash, S.A. Gaffoor, US Patent Application, 31 January, 2003.
- [35] B. Hariprakash, P. Bera, K.C. Patil, M.S. Hegde, A.K. Shukla, S.A. Gaffoor, Indian Patent Application, 24 April, 2004.
- [36] B. Hariprakash, A.U. Mane, S.K. Martha, S.A. Gaffoor, S.A. Shivashankar, A.K. Shukla, *Electrochem. Solid-State Lett.* 7 (2004) A66.
- [37] S. K. Martha, B. Hariprakash, S.A. Gaffoor, A.K. Shukla, Indian Patent Application, 16 March, 2004.
- [38] B. Hariprakash, S.K. Martha, A. Jaikumar, A.K. Shukla, *J. Power Sources* 137 (2004) 128.
- [39] B.A. Boukamp, *Equivalent-Circuit User Manual*, University of Twente, The Netherlands, 1988–1989.